Geophysical Research Letters®

AN AGU JOURNAL

Aims and Scope. *Geophysical Research Letters,* an open access journal, publishes high-impact, innovative, and timely research on major scientific advances in all the major geoscience disciplines. Papers are communications-length articles and should have broad and immediate implications in their discipline or across the geosciences. GRL maintains the fastest turn-around of all high-impact publications in the geosciences and works closely with authors to ensure broad visibility of top papers.

For submission instructions or to submit a manuscript visit: https://grl-submit.agu.org.

The journal to which you are submitting your manuscript employs a plagiarism detection system. By submitting your manuscript to this journal you accept that your manuscript may be screened for plagiarism against previously published works.

Geophysical Research Letters accepts articles for Open Access publication. Please visit https://authorservices.wiley.com/open-research/openaccess/about-wiley-open-access/index.html for further information about Open Access.

Publication Charges. The publication charge income received for *Geophysical Research Letters* helps support rapid publication, allows more articles per volume, makes possible the low subscription rates, and supports many of AGU's scientific and outreach activities. Publication charge information can be found here: https://www.agu.org/Publish-with-AGU/Publish/Author-Resources/Publication-fees. There is no charge for color in any format.

Access to this journal is available free online within institutions in the developing world through the AGORA initiative with the FAO, the HINARI initiative with the WHO, the OARE initiative with UNEP, and the ARDI ini-tiative with WIPO. For information, visit www.aginternetwork.org, www.who.int/hinari/en/, www.oaresciences.org, or www.wipo.int/ardi/en.

For submission instructions, subscription and all other information visit: http://grl.agu.org

Cover: 3D illustration of the interaction between a moon of Jupiter and its magnetospheric environment, similar to what was observed by Juno during the Europa flyby. The color scales display the magnetic field B and the plasma density n, respectively. The figure was prepared by Charles Michael Haynes.

Peter Addison, C. Michael Haynes, Aaron M. Stahl, Lucas Liuzzo, and Sven Simon contributed equally to this study.

Key Points:

- By applying a hybrid model (kinetic ions, fluid electrons), we study Europa's interaction with Jupiter's magnetosphere during the Juno flyby
- A dawn-dusk asymmetry in Europa's atmosphere can reproduce the large-scale structure of the draping signatures seen by the Juno magnetometer
- The spacecraft encountered the center of Europa's southern Alfven wing during ingress and the periphery of the northern wing during egress

Magnetic Signatures of the Interaction Between Europa and Jupiter's Magnetosphere During the Juno Flyby

Peter Addison[1] , C. Michael Haynes[1] , Aaron M. Stahl[1,2] , Lucas Liuzzo[3] , and Sven Simon[1,2]

[1]School of Earth and Atmospheric Sciences, Georgia Institute of Technology, Atlanta, GA, USA, [2]School of Physics, Georgia Institute of Technology, Atlanta, GA, USA, [3]Space Sciences Laboratory, University of California, Berkeley, Berkeley, CA, USA

Abstract Based on a hybrid model of Europa's magnetospheric interaction, we provide context for the magnetic field perturbations observed by the Juno spacecraft during its only close flyby of the moon in September 2022. By systematically varying the incident flow conditions and the density profile of Europa's atmosphere, we demonstrate that the observed, large-scale signatures of magnetic field draping are consistent with a dawn-dusk asymmetry in the moon's neutral envelope. During the flyby, such an asymmetry would have enhanced the magnetic perturbations in Europa's anti-Jovian hemisphere, explaining why the spacecraft already detected strong field line draping while still several moon radii away. Conversely, a reduced neutral density in the sub-Jovian hemisphere can explain why the perturbations in the flow-aligned field component remained nearly constant as Juno approached Europa. While a dawn-dusk asymmetry in Europa's atmosphere has been predicted by theoretical work, our results provide the first in situ hints of its presence.

Plain Language Summary Located within Jupiter's magnetosphere, the small Galilean moon Europa is continuously exposed to a flow of magnetized plasma, traveling at a relative velocity of about 100 km/s. The deflection of this plasma around Europa generates perturbations to Jupiter's magnetic field, as observed for the first time in two decades during the flyby of the Juno spacecraft in 2022. The magnitude and extension of these magnetic perturbations are largely determined by the shape of Europa's atmosphere and ionosphere which represent obstacles to the incident magnetospheric plasma. To provide three-dimensional context for the structure of Europa's magnetic environment at the time of the Juno flyby, we have applied a computer simulation to study the moon's interaction with the plasma flow. Comparison between modeled and observed magnetic fields suggests that, at the time when Juno collected these data, Europa's atmosphere may have been denser in the anti-Jovian than in the Jupiter-facing hemisphere. Theoretical predictions suggest such an asymmetry to be present in Europa's neutral envelope, partially generated by centrifugal and Coriolis forces acting on the gas molecules during the moon's rotation around Jupiter. Our study reveals first hints from a spacecraft flyby that such a hemispheric asymmetry may indeed exist in Europa's atmosphere.

1. Introduction

Europa, the smallest of Jupiter's Galilean moons (radius $R_E = 1,560.8$ km), has been visited by the Galileo spacecraft during 11 close flybys between 1996 and 2000. Magnetic field observations from these encounters revealed the presence of a time-varying, internal dipole moment at Europa that stems from currents induced within a conducting subsurface ocean (Kivelson et al., 2000; Schilling et al., 2007; Zimmer et al., 2000). Galileo also detected a strong interaction between Europa and the incident magnetospheric plasma: the moon's oxygen-rich atmosphere (e.g., Plainaki et al., 2018) is partially ionized by electron impacts (Saur et al., 1998), and newly generated ions are incorporated into the magnetospheric flow, draining momentum from it and causing its deflection around the obstacle (Kivelson et al., 2009). The induced dipole also contributes to the modification of the flow pattern and magnetospheric field near Europa (e.g., Neubauer, 1999; Volwerk et al., 2007). The impinging magnetospheric field lines pile up at Europa's ramside, forming a draping pattern and connecting to a system of Alfvén wings at larger distances to the moon (e.g., Neubauer, 1980, 1998).

To provide three-dimensional context for magnetic field data collected along the Galileo flyby trajectories, a broad pallet of models has been applied to study Europa's interaction with the Jovian magnetosphere (e.g., Arnold et al., 2019; Harris et al., 2021; Jia et al., 2018). However, currently there is no comprehensive description available that captures the structure of Europa's atmosphere for any given combination of the moon's orbital
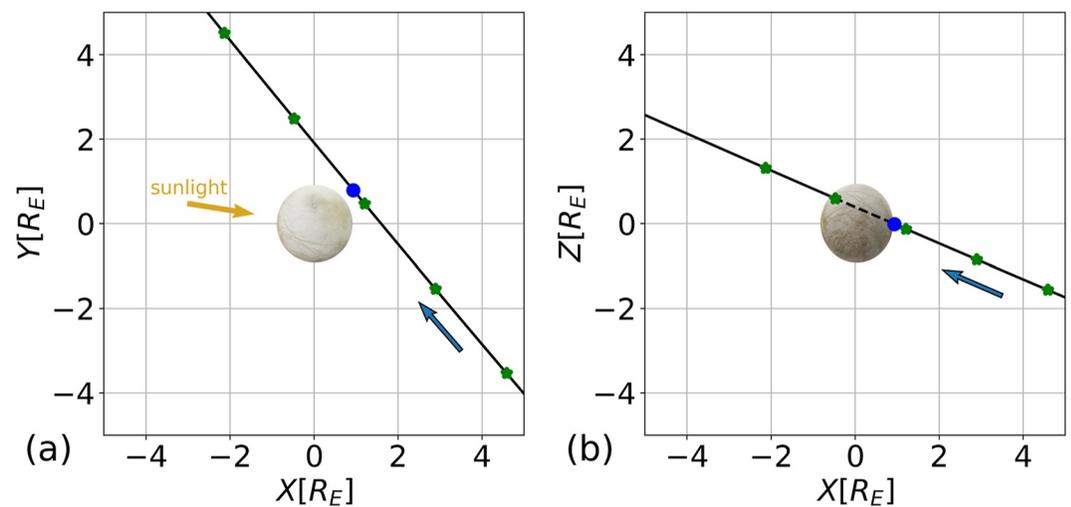
Figure 1. Trajectory of the Juno spacecraft during its close flyby of Europa on 29 September 2022. The panels display the projections of the trajectory onto the (a) $Z = 0$ and (b) $Y = 0$ planes of the EPhiO system. The blue circle represents the position of Juno's closest approach at 09:36:29 UTC. The green asterisks along the trajectory are 3 min apart, starting at 09:30:00 UTC. During the dashed portion of the trajectory in panel (b), Juno was located "behind" Europa in the $Y > 0$ half space. The blue arrow denotes Juno's direction of travel. The orange arrow in panel (a) represents the direction of the incident solar radiation.

position (defined by the Jovian Local Time) and its distance to the center of Jupiter's magnetospheric plasma sheet (defined by the System III longitude). Therefore, any such plasma interaction model inherently needs to make assumptions on potential asymmetries present in Europa's neutral gas envelope. For instance, the magneto-hydrodynamic (MHD) model of Blöcker et al. (2016) treated the moon's global O_2 atmosphere as spherically symmetric, and this symmetry is broken only by localized plumes of water vapor at various positions across the surface. The MHD models of Rubin et al. (2015), Jia et al. (2018), and Harris et al. (2021, 2022) as well as studies with the AIKEF hybrid model (e.g., Addison et al., 2021; Arnold et al., 2019) assumed a ram-wake asymmetry to be present in Europa's O_2 envelope, that is, the neutral density in these models peaks at the moon's ramside apex and is reduced in the wakeside hemisphere. This assumption is based on the notion that surface sputtering by energetic ions (a major contributor to Europa's atmosphere) is largely concentrated around the moon's ramside apex (Cassidy et al., 2013). The presence of enhanced ion sputtering rates near the ramside apex was recently put into question by Addison et al. (2021, 2022) who calculated the trajectories of the incident ener-getic ions in a realistically draped electromagnetic environment. In their recent MHD modeling study, Cervantes and Saur (2022) again treated Europa's O_2 atmosphere as spherically symmetric. These authors also included a "bulge" of enhanced H_2O density around the moon's dayside (or ramside) apex, consistent with observations by the Hubble Space Telescope (Roth, 2021).

Oza et al. (2019) developed a Monte Carlo model of O_2 dynamics in Europa's atmosphere, taking into account the moon's motion around Jupiter along its 85-hr orbit and the associated, tidally locked rotation around its polar axis. Under the assumption that O_2 is mainly generated near Europa's dayside apex, Oza et al. (2019) demonstrated the presence of a dawn-dusk asymmetry in the neutral gas density: an atmospheric "bulge" is formed in Europa's dusk hemisphere, while a corresponding reduction in column density was identified in the dawn hemisphere. Depending on surface location, the model of Oza et al. (2019) suggests O_2 column densities in the range of $(7.4 - 8.1) \cdot 10^{17} \mathrm{m}^{-2}$. The dawn-dusk asymmetry of Europa's atmosphere proposed by these authors has not yet been included in any model of the moon's plasma interaction.

On 29 September 2022, the Juno spacecraft carried out its only close flyby of Europa, reaching a closest approach altitude of 354.5 km ($0.23R_E$) at 09:36:29 UTC. Figure 1 displays the trajectory of this flyby in the Cartesian EPhiO coordinate system. The origin of this system coincides with the center of Europa. Its ($+X$) axis is aligned with the direction of corotation, and the ($+Y$) axis points toward Jupiter. The ($+Z$) axis completes the right-handed system, pointing northward. Juno approached Europa from its anti-Jovian side while traveling northward and toward upstream. However, the spacecraft remained downstream of the moon during most of the flyby. The

Table 1
AIKEF Model Parameters

Model setup	#1	#2	#3	#4	#5	#6
n_0 [cm^{-3}]	100	100	100	100	100	100
u_0 [km/s]	87	87	100	100	100	100
ϕ [°]	0	15	15	0	0	15
$\underline{B}_0$ [nT]	(77.2, −120.2, −422.0)	(77.2, −120.2, −422.0)	(77.2, −120.2, −422.0)	(77.2, −120.2, −422.0)	(77.2, −120.2, −422.0)	(77.2, −120.2, −422.0)
$\left|\underline{B}_0\right|$ [nT]	445.5	445.5	445.5	445.5	445.5	445.5
$\underline{M}_{\text{ind}}$ [· 10^{18} J/T]	(−1.4, 2.0, 0)	(−1.4, 2.0, 0)	(−1.4, 2.0, 0)	(−1.4, 2.0, 0)	(−1.4, 2.0, 0)	(-1.4, 2.0, 0)
β_i	$4.6 \cdot 10^{-2}$	$4.6 \cdot 10^{-2}$	$4.6 \cdot 10^{-2}$	$4.6 \cdot 10^{-2}$	$4.6 \cdot 10^{-2}$	$4.6 \cdot 10^{-2}$
β_e	$4.6 \cdot 10^{-2}$	$4.6 \cdot 10^{-2}$	$4.6 \cdot 10^{-2}$	$4.6 \cdot 10^{-2}$	$4.6 \cdot 10^{-2}$	$4.6 \cdot 10^{-2}$
$|\underline{v}_{A,0}|$ [km/s]	225.9	225.9	225.9	225.9	225.9	225.9
M_A	0.39	0.39	0.44	0.44	0.44	0.44
M_S	1.9	1.9	2.20	2.20	2.20	2.20
M_{MS}	0.38	0.38	0.43	0.43	0.43	0.43
n_0 [m^{-3}]	$5 \cdot 10^{13}$	$5 \cdot 10^{13}$	$5 \cdot 10^{13}$	$5 \cdot 10^{13}$	$5 \cdot 10^{13}$	$5 \cdot 10^{13}$
H [km]	100	100	100	100	100	100
λ	5	5	5	–	–	5
A	–	–	–	10	0	–
Bulge location	Anti-Jovian (20° N)	Anti-Jovian (20° N)	Anti-Jovian (20° N)	Ramside	–	anti-Jovian

Note. Values of the plasma beta $\beta_s = \frac{2\mu_0 n_0 k_B T_s}{B_0^2}$ are computed for magnetospheric ions (index $s = i$) and electrons ($s = e$) separately, using temperatures T_s from Kivelson et al. (2004). The magnitude of the Alfvén velocity $\underline{v}_{A,0} = \frac{B_0}{\sqrt{\mu_0 m_0 n_0}}$ as well as the Alfvénic (M_A), sonic (M_S), and magnetosonic (M_{MS}) Mach numbers are also given.

encounter occurred at a Jovian Local Time of 18:40, that is, the direction of the incident magnetospheric plasma was nearly aligned with the Sun-Europa line (see Figure 1b in Liuzzo et al. (2015)). In other words, Europa's dusk terminator was located in the anti-Jovian half space ($Y < 0$), approximately 90° in longitude eastward of the subsolar point. For this reason, Europa's location during the Juno flyby facilitates the search for any dawn-dusk asymmetries in the plasma interaction region which, in turn, may provide hints of similar hemispheric dichotomies in the moon's neutral envelope.

In this letter, we analyze the time series recorded by Juno's magnetometer (Connerney et al., 2017) during the Europa flyby. By applying the AIKEF hybrid model (Müller et al., 2011), we demonstrate that a dawn-dusk asymmetry in the moon's atmosphere provides a possible explanation for the magnetic perturbations observed along the Juno trajectory.

2. Application of the AIKEF Hybrid Model to Europa

The AIKEF model treats ions as individual macroparticles, whereas electrons form a massless, charge-neutralizing fluid. The model has an extensive history of applications to Europa's plasma interaction (Addison et al., 2021, 2022; Addison, Liuzzo, & Simon, 2023; Arnold et al., 2019; Arnold, Liuzzo, & Simon, 2020; Arnold, Simon, & Liuzzo, 2020; Breer et al., 2019; Haynes et al., 2023). To study Europa's environment during the Juno flyby, we carried out over 60 model runs, systematically varying the incident magnetospheric flow conditions and the structure of the moon's atmosphere. This letter discusses results from six of these setups (see Table 1) which were found to be most instructive for the interpretation of Juno magnetometer observations. These six runs assume the ion population of the impinging thermal plasma to consist of a singly charged species with mass $m_0 = 18.5$ amu (analogous to, e.g., Addison et al., 2021, 2022) and number density $n_0 = 100$ cm^{-3}. This value is (approximately) the average between the densities obtained from the empirical models of Bagenal and Delamere (2011) and Roth et al. (2014) for Europa's system III longitude during the flyby ($\lambda_{III} = 136°$). At the time of this writing, ambient plasma moments from the Juno flyby were not yet available in the peer-reviewed literature.

The bulk velocity of the impinging flow is set to $\left|\underline{u}_0\right| = 87\,\text{km/s}$ (setups #1 and #2) or $\left|\underline{u}_0\right| = 100\,\text{km/s}$ (setups #3–#6), which is within the range of velocity magnitudes deduced from Galileo observations (Bagenal & Dols, 2020). In setups #1, #4, and #5, the upstream flow travels along the ($+X$) direction, while setups #2, #3, and #6 take into account the small radial flow component observed near Europa's orbital distance (Bagenal et al., 2016): in these two configurations, the flow vector $\underline{u}_0 = u_0(\cos\phi, \sin\phi, 0)$ is inclined toward Jupiter by $\phi = 15°$. This tilt may be caused by radial plasma transport in the Jovian magnetosphere and the angle is within the range covered by the error bars in Figure 5 of Bagenal et al. (2016). The uniform background magnetic field $\underline{B}_0$ is the same in all six setups and was obtained by interpolating the magnetospheric field observed before entering and after exiting Europa's interaction region (see Section 3) to the point of Juno's closest approach. Taking into account Equation 2 from Addison et al. (2021), the vector $\underline{B}_0$ also determines the moon's induced magnetic moment $\underline{M}_{\text{ind}}$ at the time of the flyby. We use a cuboid-shaped domain with extensions of $-8R_E \leq X \leq 22R_E$, $-10R_E \leq Y \leq 10R_E$, $-30R_E \leq Z \leq 30R_E$.

A critical input parameter for our model is the shape of Europa's atmosphere, which is partially ionized by electron impacts to form the moon's ionosphere (see, e.g., Arnold et al. (2019) for details). Unlike preceding studies with AIKEF (e.g., Addison et al., 2021, 2022), setups #1–#3 and #6 no longer include an enhancement in the neutral density near Europa's ramside apex and an associated decrease in density around the wakeside apex. Instead, we describe the neutral profile n_n with the expression

$$n_n(h, \psi, \lambda) = \begin{cases} n_0 \left[\cos\left(\frac{\psi}{2}\right)\right]^\lambda \exp\left(\frac{R_E - r}{H}\right) & : \quad \psi \leq 170° \\ n_0 \left[\cos\left(\frac{170°}{2}\right)\right]^\lambda \exp\left(\frac{R_E - r}{H}\right) & : \quad \psi > 170° \end{cases}, \tag{1}$$

where $r = \sqrt{X^2 + Y^2 + Z^2}$ is the distance to the moon's center and H is the atmospheric scale height. The parameter ψ denotes the angle between the vector $\underline{r} = (X, Y, Z)$ and a fixed radial unit vector $\underline{e}$, pointing from the center of Europa toward a point on the moon's surface. The profile defined by Equation 1 is axially symmetric around the direction of $\underline{e}$, producing a bulge in number density at $\psi = 0°$ and a minimum for $\psi \geq 170°$. The exponent λ in Equation 1 is used to define the "steepness" of the decrease in atmospheric density with growing angular distance ψ from the bulge. A slightly modified form of Equation 1 was used by Liuzzo et al. (2015) to emulate asymmetries in Callisto's neutral envelope.

In our setup #6, the location of the atmospheric bulge is defined by $\underline{e} = (0, -1, 0)$, that is, it coincides with the moon's anti-Jovian apex. The Juno flyby occurred around 18:40 Jovian Local Time; that is, Europa's duskside apex was displaced by about $10°$ in longitude away from the $X = 0$ plane and toward the solar apex. However, Figure 4 of Oza et al. (2019) shows that their atmospheric density maximum does not occur precisely along the semi-meridian at dusk, but is slightly displaced toward the nightside by $10° - 15°$ in longitude. These two longitudinal displacements (one toward the dayside, the other toward the nightside apex) approximately compensate each other. For our study of the Juno flyby, we therefore center the atmospheric bulge around Europa's anti-Jovian apex.

Addison et al. (2021) demonstrated that a non-zero $B_{0,X}$ component of the magnetospheric background field breaks the symmetry of energetic ion precipitation onto the moon's surface between its northern and southern hemispheres. The "Case (1)" scenario studied by these authors includes a *negative* $B_{0,X}$ component, and it was revealed that this tilt of $\underline{B}_0$ toward upstream leads to slightly elevated influx of magnetospheric ions onto Europa's *southern* hemisphere. Conversely, the *positive* $B_{0,X}$ component observed during the Juno flyby (see Table 1) corresponds to enhanced magnetospheric ion precipitation onto Europa's *northern* hemisphere. For this reason, we also explored several configurations with the atmospheric density bulge located along the moon's anti-Jovian semi-meridian, but slightly displaced toward the north: in our setups #1–#3, the location of the atmospheric density peak is defined by $\underline{e} = (0, -\cos 20°, +\sin 20°)$, that is, it is rotated northward by $20°$ within the $X = 0$ plane. We emphasize that Addison et al. (2021) did *not* provide a conversion of their modeled ion influx patterns into actual atmospheric density profiles. In this sense, scenarios #1–#3 assume that the north-south asymmetry seen by Addison et al. (2021) in ion precipitation patterns likewise maps into the resulting atmospheric density profile. However, this assumption is currently heuristic in nature and does not follow from rigorous quantitative modeling of Europa's neutral envelope. For all setups discussed here, the values of the atmospheric scale

height and the "steepness parameter" have been set to $H = 100$ km (see, e.g., Addison et al., 2021, 2022; Haynes et al., 2023) and $\lambda = 5$, respectively. Neither parameter was found to have significant influence on the conclusions drawn.

In addition, we have carried out simulations to demonstrate that the atmospheric profiles used in earlier modeling studies are *not* suitable to explain the magnetic signatures observed by Juno. Setup #4 includes a ram-wake asymmetry in the neutral density, using Equation 1 from Arnold et al. (2019) and adopting their value of $A = 10$ for the "asymmetry parameter": the density at Europa's ramside apex then exceeds that at the wakeside apex by a factor of $A + 1 = 11$. In setup #5, Europa's neutral envelope is treated as spherically symmetric (analogous to, e.g., Blöcker et al., 2016), that is, A is set to zero. In all six model setups, Europa's atmosphere is assumed to consist of O_2 only, that is, we include neither transient plumes of water vapor (Arnold et al., 2019; Jia et al., 2018) nor a bulge of H_2O molecules around the subsolar or dayside apex (Roth, 2021). Each of these additional atmospheric components was found to generate only very localized perturbations to the magnetic field on length scales much smaller than the extension of the signatures observed by Juno (e.g., Cervantes & Saur, 2022; Haynes et al., 2023). The surface density n_0 in all six setups is chosen such that the column density n_0H is of the same order ($\approx 10^{18}$ m^{-2}) as derived from remote observations (see, e.g., Addison et al., 2021 for details) and proposed by Oza et al. (2019).

3. Juno Magnetometer Observations and Model Results

In Figure 2 we display Juno magnetic field observations from the Europa flyby as well as the synthetic time series from the six AIKEF runs. We also show (in plot (b)) the magnetic signature obtained by taking the sum of $\underline{B}_0$ and the induced field from Europa's subsurface ocean. This setup assumes the moon's environment to be devoid of any plasma currents. Juno's closest approach to Europa approximately coincided with the spacecraft's passage through the $Z = 0$ plane as it traveled from southern to northern latitudes. The geometry of Europa's plasma interaction during this flyby is somewhat tricky to capture, since $\underline{B}_0$ possesses three non-vanishing components. This implies that, for example, none of the three planes of the EPhiO system represents a symmetry plane between the moon's northern ($-$) and southern ($+$) Alfvén wing characteristics $\underline{\mathcal{Z}}_{\pm} = \underline{u}_0 \pm \underline{v}_{A,0}$ (Neubauer, 1980). Besides, while Europa's induced dipole moment is still contained within the $Z = 0$ plane, it is inclined by 33° against the Y axis.
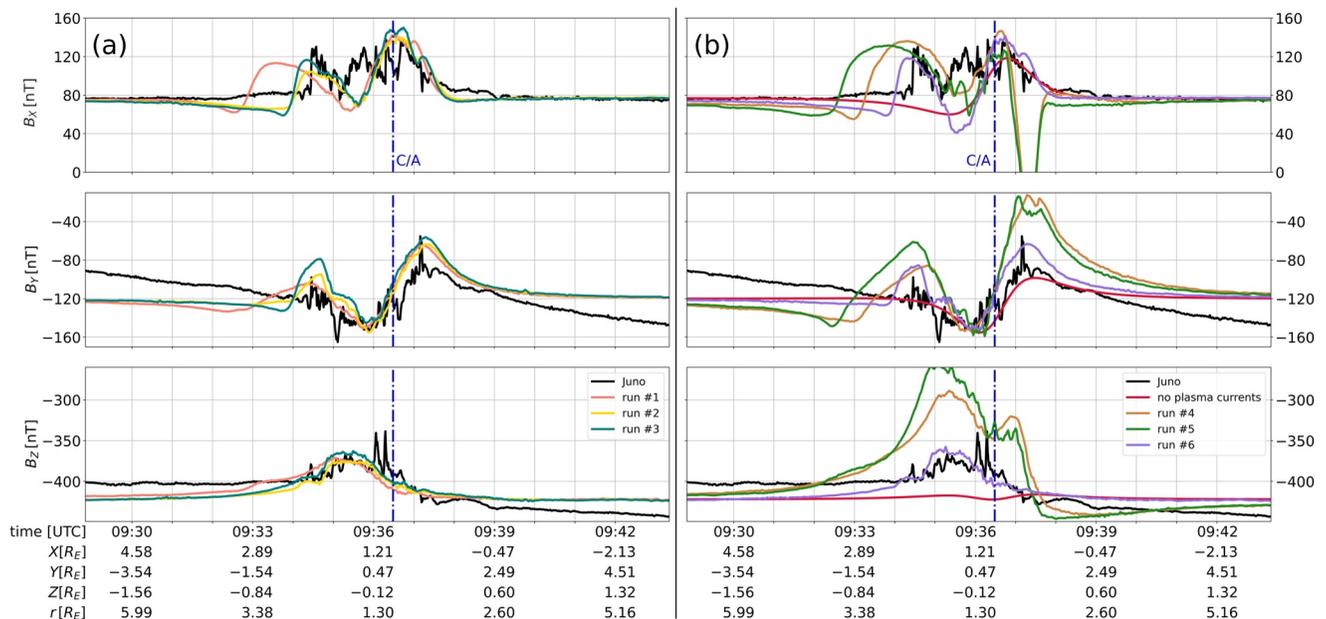
Figure 2. Magnetic field $\underline{B} = (B_X, B_Y, B_Z)$ near Europa in EPhiO coordinates: model results versus Juno data. The figure displays time series of the observed magnetic field components (black) as well as output from AIKEF runs (a) #1–#3 and (b) #4–#6. Plot (b) also shows the magnetic field obtained from a mere superposition of $\underline{B}_0$ and Europa's induced dipole (red). The dash-dotted blue line (labeled C/A) denotes the position of Juno's closest approach.

As shown in Figure 2, the observed B_X component exhibits a broad enhancement, commencing in Europa's southern hemisphere around 09:34 UTC and reaching up to $Z = +0.6R_E$ into the northern hemisphere (until 09:39 UTC). The occurrence of positive perturbations δB_X (where $\delta B_i = B_i - B_{0,i}$ for $i = X, Y, Z$) on *both* sides of Europa's equatorial plane is not unexpected: due to the tilt of $\underline{B}_0$ toward downstream ($B_{0,X} > 0$, see Table 1), the Alfvén characteristics are rotated counter-clockwise around the ($+Y$) axis, allowing the southern wing tube (where $\delta B_X > 0$) to penetrate into the northern half space (e.g., Simon and Motschmann (2009)). Likewise, the northern wing is rotated away from Juno's trajectory, causing the spacecraft to entirely miss the region of $\delta B_X < 0$ associated with $\underline{Z}_-$. Europa's induced dipole alone also generates perturbations $\delta B_X > 0$ above the $Z = 0$ plane (red in Figure 2b). In setups that include the atmospheric bulge in Europa's anti-Jovian hemisphere (#1–#3 and #6), this B_X enhancement is further amplified by the plasma interaction.

While the B_X perturbations seen by Juno (black) remained positive throughout the encounter, the strength δB_X of this enhancement changed non-monotonically with time, achieving a broad local minimum in Europa's southern hemisphere around 09:35 UTC. The subsequent B_X enhancement is "interrupted" by several smaller dips, but these are way less prominent than the feature observed around 09:35. The large-scale shape of the modeled B_X in setups #1–#3 ("enhancement-dip-enhancement") is similar to the observed signature. However, the locations of the modeled, large-scale B_X features do not precisely coincide with observations. In these three runs, the central dip is displaced slightly toward upstream: around 09:35:30, AIKEF output still displays the dip while observations show that Juno had already entered the outbound enhancement. These deviations may stem from uncertainties in the atmosphere parameters. The smaller dips imposed on the outbound enhancement are likely caused by fine structures in Europa's ionosphere which the model is not designed to resolve. In setup #1 (which uses $\phi = 0°$), the onset of the modeled B_X increase occurs about 90 s earlier than observed, corresponding to a distance of $1.3R_E$ traveled along Juno's trajectory. However, setups #2 and #3 almost precisely match the observed location and width of the B_X enhancement. The slight tilt of $\underline{u}_0$ toward Jupiter in the latter two setups rotates the Alfvén characteristics into the Jupiter-facing half space. Juno approached Europa from the anti-Jovian side; this implies that in setups #2 and #3 the spacecraft would enter the region of draped field lines later than in setup #1.

Setup #6 (see Figure 2b) includes less "fine-tuning" than configurations #2–#3: the atmospheric bulge coincides precisely with Europa's anti-Jovian apex. Nevertheless, the model still matches both the locations and the magnitudes of the two spikes associated with the asymmetric B_X signature. However, setup #6 overestimates the reduction near the inbound edge of the B_X feature, with the modeled δB_X clearly turning negative. This run still emphasizes the "robustness" of our conclusions, illustrating that the notion of a dawn-dusk asymmetry in Europa's atmosphere during the Juno flyby can qualitatively explain the shape of the observed B_X perturbations over a broad range of upstream and atmospheric parameters.

Setups #4 and #5 do not include an atmospheric bulge in the anti-Jovian hemisphere. The magnetic signatures obtained from these runs reveal significant qualitative differences to Juno observations. First, the onset of the inbound B_X enhancement occurs earlier than detected. Analogous to our discussion of setups #1–#3, this displacement may again be reduced by including a small component of $\underline{u}_0$ along ($+Y$). Second, and more importantly, runs #4 and #5 both reveal a region of *negative* B_X in the outbound segment of the flyby, corresponding to a passage through the center of Europa's northern Alfvén wing tube in the $Z > 0$ half space. Additional simulations suggested that this $B_X < 0$ feature cannot be eliminated by tilting the upstream flow vector within the observational bounds from Bagenal et al. (2016). The only way we found to prevent Juno's trajectory from intersecting the $B_X < 0$ region is a localized reduction of the atmospheric column density near Europa's sub-Jovian apex by several orders of magnitude, as realized by Equation 1. Using such a low column density ($\approx 2.5 \cdot 10^{13}$ m^{-2}) *uniformly* across Europa's entire neutral envelope would be inconsistent with magnetometer observations: in this case, the modeled B_X would be very similar to the "superposition case" (red) that does not include plasma effects. Hence, the observed B_X perturbations support the notion of Europa's atmosphere at the time of the flyby having been more dense in the anti-Jovian than in the sub-Jovian hemisphere. Such an asymmetric configuration can explain why Juno encountered a strong increase in B_X while traveling through the anti-Jovian half space and still several R_E downstream of the moon: the locally enhanced atmospheric density causes the draping to be stronger for $Y < 0$. Besides, this atmosphere model can explain why the B_X enhancement observed close to Europa for $Y > 0$ is comparable in strength to the inbound feature seen farther downstream: the reduced atmospheric density in the $Y > 0$ half space locally weakens the plasma interaction; that is, despite the proximity to Europa the draping signature is not amplified.

The shape of the $\delta B_Y < 0$ perturbation observed shortly before closest approach can already be matched by the superposition of $\underline{B}_0$ and Europa's induced field (Figure 2b). The four setups including a dawn-dusk asymmetry in the atmosphere (#1–#3 and #6) largely reproduce the width and magnitude of the observed B_Y signature (Figure 2). These runs predict a broad enhancement $\delta B_Y > 0$ in the outbound segment, centered around the isolated $B_Y > 0$ spike seen by Juno at 09:37 UTC. The magnitude of the modeled feature matches the peak value of the observed signature ($B_Y \approx -57$ nT), while its width is overestimated. Therefore, it remains elusive whether this spike is related to Europa's plasma interaction or is magnetospheric in origin. The time series from runs #4 and #5 overestimate the strength and, especially, the width of the observed perturbations δB_Y. Particularly in the outbound region, an atmosphere with high column densities generates $\delta B_Y > 0$ signatures that are still discernible around 09:40 UTC, while the observed B_Y already returns to the Jovian background field at 09:37 UTC. This again suggests that, during the Juno flyby, the "strength" of Europa's plasma interaction (e.g., Simon et al., 2021) in the sub-Jovian hemisphere may have been locally weakened.

The observed B_Z component reveals a broad depletion feature (i.e., $\delta B_Z > 0$) around closest approach, commencing at 09:34 UTC. Such a depression region has already been identified in earlier studies of Europa's interaction (e.g., Arnold, Liuzzo, & Simon, 2020): the elevated plasma pressure associated with pick-up ions partially pushes the magnetospheric field lines out of the tail region. Analogous to B_Y, the width and magnitude of the B_Z feature can be reproduced *only* by runs that include a dawn-dusk asymmetry of Europa's neutral envelope. None of our modeled time series reproduce the double-spike signature observed in B_Z shortly before closest approach. This may indicate that the representation of the ionosphere in AIKEF does not include sufficient complexity to reproduce such fine structures.

To provide some context for the qualitative differences in the modeled B_X signatures, Figure 3 displays two-dimensional profiles of this component in the three planes of the EPhiO system. The left column illustrates results from setup #2 (which does not produce a $\delta B_X < 0$ segment after Juno's closest approach), while the right column shows output from run #4 (which suggests $\delta B_X < 0$ in the outbound region). As can be seen from the top and middle rows, Europa's Alfvén wings are rotated toward Jupiter around the Z axis and northward around the Y axis. The bottom row in Figure 3 reveals the reason for the morphological differences in B_X along the Juno trajectory. In run #2, the core of the northern Alfvén wing ($\delta B_X < 0$, blue) is shifted slightly toward the $Y < 0$ half space where the atmospheric density is larger. This happens despite the inclusion of a small upstream flow component *toward* Jupiter. The "ray" of $\delta B_X > 0$ in the northern, Jupiter-facing half space (red in panel 3(e)) corresponds to the outer region of the $\underline{\mathcal{Z}}_-$ wing: in planes perpendicular to $\underline{\mathcal{Z}}_\pm$, the magnetic perturbations associated with an Alfvén wing can be represented by a two-dimensional dipole (Neubauer, 1980); that is, the field lines need to *close* outside of the core region. Therefore, the field lines inside the northern wing tube are draped ($\delta B_X < 0$), but in the periphery of the wing they appear "anti-draped" ($\delta B_X > 0$).

In setup #2, the "thinning" of the northern wing tube for $Y > 0$ caused Juno to first travel through the center of the southern wing tube (where the field is draped, $\delta B_X > 0$), and then graze the outer regions of the northern wing where the field is "anti-draped." For this reason, the observed δB_X in the north has the *same* sign as in the south. In setup #4, the northern wing tube (characterized by $\delta B_X < 0$, blue) extends slightly farther toward Jupiter than in setup #2 (panels 3(f) versus (e)). Therefore, in run #4 Juno would have encountered the center of the northern wing as it traveled through the $Z > 0$ half space. However, this picture is incompatible with observations.

4. Concluding Remarks

Results from the AIKEF model suggest that reproducing the large-scale shape and magnitude of the magnetic perturbations observed during Juno's Europa flyby requires the inclusion of a dawn-dusk asymmetry in the moon's neutral envelope. Within our model, neither a spherically symmetric atmosphere nor the notion of a ram-wake asymmetry can reproduce the overall shape and strength of the signatures seen by Juno. However, this interpretation of the magnetic perturbations is possibly not unique, as we have explored only a small corner of the parameter space spanned by the upstream flow parameters and the neutral density profile. Various fine structures in the observed magnetic field are not reproduced by any of the analyzed model setups. In addition, Juno was still several R_E downstream when traveling through Europa's anti-Jovian hemisphere; that is, a potential atmospheric bulge around dusk was not directly sampled. Magnetometer and particle data from additional close flybys in Europa's dusk and dawn hemispheres are needed to further substantiate the presence of such an atmospheric asymmetry.
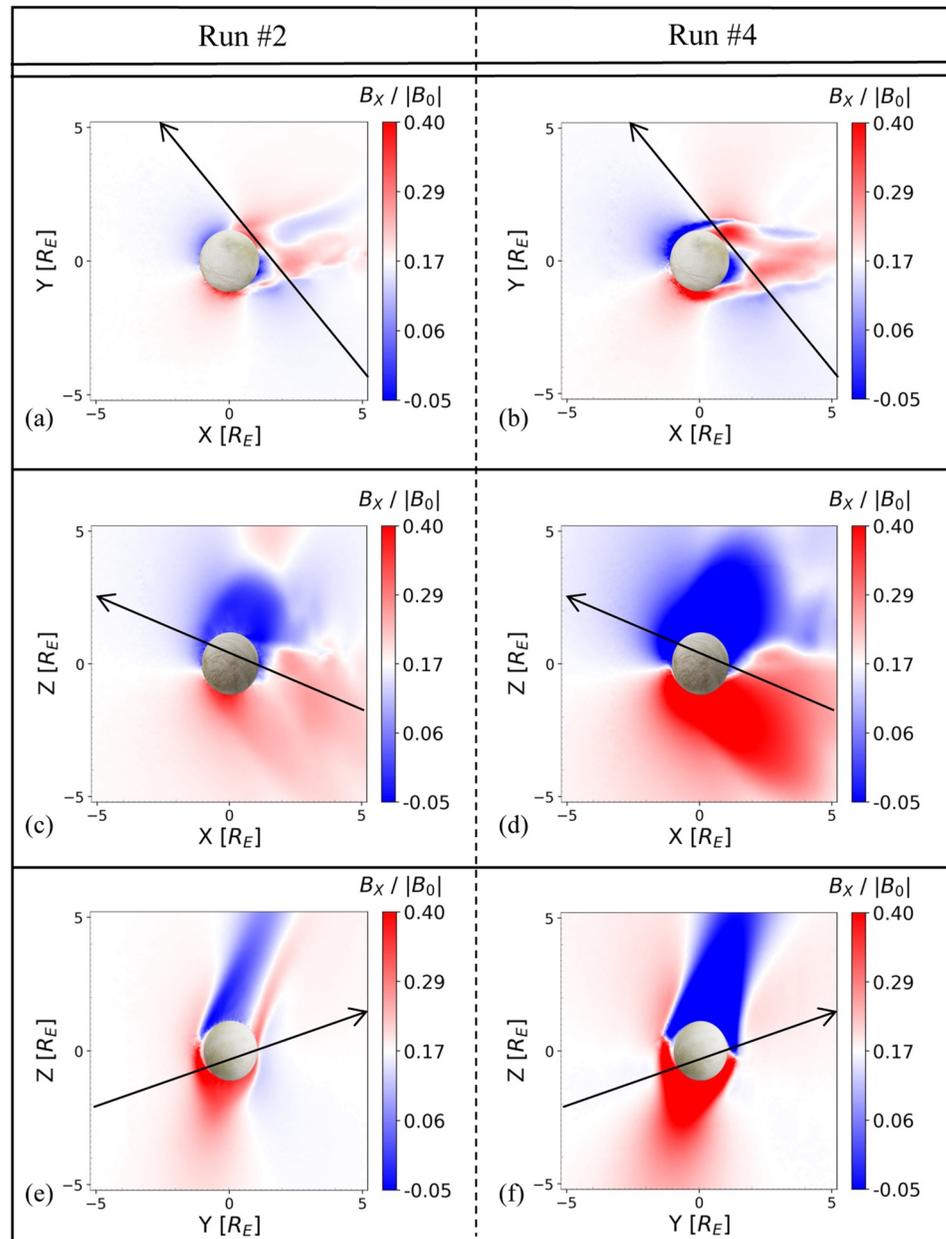
Figure 3. Modeled B_X components in the $Z = 0$ (panels (a) and (b)), $Y = 0$ (panels (c) and (d)), and $X = 0$ planes (panels (e) and (f)). Results from setup #2 are displayed in the left column, whereas the right column shows output from run #4. In all panels, white coloring corresponds to the $B_{0,X}$ component of the magnetospheric background field. The projection of Juno's trajectory onto each cutting plane is indicated by the black line.

The minimum atmospheric density at the sub-Jovian apex used in our model is by orders of magnitude lower than proposed by Oza et al. (2019). However, the concentration of surface sputtering around Europa's dayside apex assumed by these authors is inconsistent with more recent results that take into account the deflection of impinging magnetospheric particles by the draped fields (Addison et al., 2022; Addison, Liuzzo, & Simon, 2023). Therefore, future search for dawn-dusk asymmetries in Europa's atmosphere will need to combine the approach of Oza et al. (2019)—including the moon's rotation when calculating atmospheric dynamics—with a more accurate distribution of magnetospheric ion and electron sputtering across the surface.

Data Availability Statement

Output from the AIKEF model and Juno magnetometer data used for comparison have been archived by Addison, Haynes, et al. (2023). Juno magnetometer data are publicly available at the NASA Planetary Data System (Connerney, 2022).

References

Addison, P., Haynes, C. M., Stahl, A., Liuzzo, L., & Simon, S. (2023). Data for "Magnetic Signatures of the Interaction Between Europa and Jupiter's Magnetosphere during Juno's Close Flyby" by Addison et al., 2023 [Dataset]. Zenodo. https://doi.org/10.5281/zenodo.8411734

Addison, P., Liuzzo, L., Arnold, H., & Simon, S. (2021). Influence of Europa's time-varying electromagnetic environment on magnetospheric ion precipitation and surface weathering. *Journal of Geophysical Research: Space Physics*, *126*(5), e2020JA029087. https://doi.org/10.1029/2020JA029087

Addison, P., Liuzzo, L., & Simon, S. (2022). Effect of the magnetospheric plasma interaction and solar illumination on ion sputtering of Europa's surface ice. *Journal of Geophysical Research: Space Physics*, *127*(2), e2021JA030136. https://doi.org/10.1029/2021JA030136

Addison, P., Liuzzo, L., & Simon, S. (2023). Surface-plasma interactions at Europa in draped magnetospheric fields: The contribution of energetic electrons to energy deposition and sputtering. *Journal of Geophysical Research: Space Physics*, *128*(8), e2023JA031734. https://doi.org/10.1029/2023JA031734

Arnold, H., Liuzzo, L., & Simon, S. (2019). Magnetic signatures of a plume at Europa during the Galileo E26 flyby. *Geophysical Research Letters*, *46*(3), 1149–1157. https://doi.org/10.1029/2018GL081544

Arnold, H., Liuzzo, L., & Simon, S. (2020). Plasma interaction signatures of plumes at Europa. *Journal of Geophysical Research: Space Physics*, *125*(1), e2019JA027346. https://doi.org/10.1029/2019JA027346

Arnold, H., Simon, S., & Liuzzo, L. (2020). Applying ion energy spectrograms to search for plumes at Europa. *Journal of Geophysical Research: Space Physics*, *125*(9), e2020JA028376. https://doi.org/10.1029/2020JA028376

Bagenal, F., & Delamere, P. A. (2011). Flow of mass and energy in the magnetospheres of Jupiter and Saturn. *Journal of Geophysical Research: Space Physics*, *116*(A5), A05209. https://doi.org/10.1029/2010JA016294

Bagenal, F., & Dols, V. (2020). The space environment of io and Europa. *Journal of Geophysical Research: Space Physics*, *125*(5), e27485. https://doi.org/10.1029/2019JA027485

Bagenal, F., Wilson, R. J., Siler, S., Paterson, W. R., & Kurth, W. S. (2016). Survey of Galileo plasma observations in Jupiter's plasma sheet. *Journal of Geophysical Research: Planets*, *121*(5), 871–894. https://doi.org/10.1002/2016JE005009

Blöcker, A., Saur, J., & Roth, L. (2016). Europa's plasma interaction with an inhomogeneous atmosphere: Development of Alfvén winglets within the Alfvén wings. *Journal of Geophysical Research: Space Physics*, *121*(10), 9794–9828. https://doi.org/10.1002/2016JA022479

Breer, B. R., Liuzzo, L., Arnold, H., Andersson, P. N., & Simon, S. (2019). Energetic ion dynamics in the perturbed electromagnetic fields near Europa. *Journal of Geophysical Research: Space Physics*, *124*(9), 7592–7613. https://doi.org/10.1029/2019JA027147

Cassidy, T., Paranicas, C., Shirley, J., Dalton, J., III, Teolis, B., Johnson, R., et al. (2013). Magnetospheric ion sputtering and water ice grain size at Europa. *Planetary and Space Science*, *77*, 64–73. https://doi.org/10.1016/j.pss.2012.07.008

Cervantes, S., & Saur, J. (2022). Constraining Europa's subsolar atmosphere with a joint analysis of HST spectral images and Galileo magnetic field data. *Journal of Geophysical Research: Space Physics*, *127*(9), e30472. https://doi.org/10.1002/jgra.v127.9

Connerney, J. E. P. (2022). Juno MAG CALIBRATED DATA J V1.0, JNO-J-3-FGM-CAL-V1.0 [Dataset]. NASA Planetary Data System. https://doi.org/10.17189/1519711

Connerney, J. E. P., Benn, M., Bjarno, J. B., Denver, T., Espley, J., Jorgensen, J. L., et al. (2017). The Juno magnetic field investigation. *Space Science Reviews*, *213*(1–4), 39–138. https://doi.org/10.1007/s11214-017-0334-z

Harris, C. D. K., Jia, X., & Slavin, J. A. (2022). Multi-fluid MHD simulations of Europa's plasma interaction: Effects of variation in Europa's atmosphere. *Journal of Geophysical Research: Space Physics*, *127*(9), e2022JA030569. https://doi.org/10.1029/2022JA030569

Harris, C. D. K., Jia, X., Slavin, J. A., Toth, G., Huang, Z., & Rubin, M. (2021). Multi-fluid MHD simulations of Europa's plasma interaction under different magnetospheric conditions. *Journal of Geophysical Research: Space Physics*, *126*(5), e2020JA028888. https://doi.org/10.1029/2020JA028888

Haynes, C. M., Tippens, T., Addison, P., Liuzzo, L., Poppe, A. R., & Simon, S. (2023). Emission of energetic neutral atoms from the magnetosphere-atmosphere interactions at Callisto and Europa. *Journal of Geophysical Research: Space Physics*, *128*(10), e2023JA031931. https://doi.org/10.1029/2023JA031931

Jia, X., Kivelson, M. G., Khurana, K. K., & Kurth, W. S. (2018). Evidence of a plume on Europa from Galileo magnetic and plasma wave signatures. *Nature Astronomy*, *2*(6), 459–464. https://doi.org/10.1038/s41550-018-0450-z

Kivelson, M. G., Bagenal, F., Kurth, W. S., Neubauer, F. M., Paranicas, C., & Saur, J. (2004). Magnetospheric interactions with satellites. In F. Bagenal, T. E. Dowling, & W. B. McKinnon (Eds.), *Jupiter. The planet, satellites and magnetosphere* (pp. 513–536). Cambridge University of Press.

Kivelson, M. G., Khurana, K. K., Russell, C. T., Volwerk, M., Walker, R. J., & Zimmer, C. (2000). Galileo magnetometer measurements: A stronger case for a subsurface ocean at Europa. *Science*, *289*(5483), 1340–1343. https://doi.org/10.1126/science.289.5483.1340

Kivelson, M. G., Khurana, K. K., & Volwerk, M. (2009). In R. T. Pappalardo, W. B. McKinnon, & K. K. Khurana (Eds.), *Europa's interaction with the Jovian magnetosphere* (p. 545). Europa.

Liuzzo, L., Feyerabend, M., Simon, S., & Motschmann, U. (2015). The impact of Callisto's atmosphere on its plasma interaction with the Jovian magnetosphere. *Journal of Geophysical Research: Space Physics*, *120*(11), 9401–9427. https://doi.org/10.1002/2015JA021792

Müller, J., Simon, S., Motschmann, U., Schüle, J., Glassmeier, K., & Pringle, G. J. (2011). A.I.K.E.F.: Adaptive hybrid model for space plasma simulations. *Computer Physics Communications*, *182*(4), 946–966. https://doi.org/10.1016/j.cpc.2010.12.033

Neubauer, F. M. (1980). Nonlinear standing Alfven wave current system at Io - Theory. *Journal of Geophysical Research*, *85*(A3), 1171–1178. https://doi.org/10.1029/JA085iA03p01171

Neubauer, F. M. (1998). The sub-Alfvénic interaction of the Galilean satellites with the Jovian magnetosphere. *Journal of Geophysical Research*, *103*(E9), 19843–19866. https://doi.org/10.1029/97JE03370

Neubauer, F. M. (1999). Alfvén wings and electromagnetic induction in the interiors: Europa and Callisto. *Journal of Geophysical Research: Space Physics*, *104*(A12), 28671–28684. https://doi.org/10.1029/1999JA900217

Oza, A. V., Leblanc, F., Johnson, R. E., Schmidt, C., Leclercq, L., Cassidy, T. A., & Chaufray, J.-Y. (2019). Dusk over dawn O_2 asymmetry in Europa's near-surface atmosphere. *Planetary and Space Science*, *167*, 23–32. https://doi.org/10.1016/j.pss.2019.01.006

Plainaki, C., Cassidy, T. A., Shematovich, V. I., Milillo, A., Wurz, P., Vorburger, A., et al. (2018). Towards a global unified model of Europa's Tenuous atmosphere. *Space Science Reviews*, *214*(1), 40. https://doi.org/10.1007/s11214-018-0469-6

Roth, L. (2021). A stable H2O atmosphere on Europa's trailing hemisphere from HST images. *Geophysical Research Letters*, *48*(20), e2021GL094289. https://doi.org/10.1029/2021GL094289

Roth, L., Retherford, K. D., Saur, J., Strobel, D. F., Feldman, P. D., McGrath, M. A., & Nimmo, F. (2014). Orbital apocenter is not a sufficient condition for HST/STIS detection of Europa's water vapor aurora. *Proceedings of the National Academy of Sciences of the United States of America*, *111*(48), E5123–E5132. https://doi.org/10.1073/pnas.1416671111

Rubin, M., Jia, X., Altwegg, K., Combi, M. R., Daldorff, L. K. S., Gombosi, T. I., et al. (2015). Self-consistent multifluid MHD simulations of Europa's exospheric interaction with Jupiter's magnetosphere. *Journal of Geophysical Research: Space Physics*, *120*(5), 3503–3524. https://doi.org/10.1002/2015JA021149

Saur, J., Strobel, D. F., & Neubauer, F. M. (1998). Interaction of the jovian magnetosphere with Europa: Constraints on the neutral atmosphere. *Journal of Geophysical Research*, *103*(E9), 19947–19962. https://doi.org/10.1029/97JE03556

Schilling, N., Neubauer, F. M., & Saur, J. (2007). Time-varying interaction of Europa with the Jovian magnetosphere: Constraints on the conductivity of Europa's subsurface ocean. *Icarus*, *192*(1), 41–55. https://doi.org/10.1016/j.icarus.2007.06.024

Simon, S., Liuzzo, L., & Addison, P. (2021). Role of the ionospheric conductance profile in sub-alfvénic moon-magnetosphere interactions: An analytical model. *Journal of Geophysical Research: Space Physics*, *126*(7), e2021JA029191. https://doi.org/10.1029/2021JA029191

Simon, S., & Motschmann, U. (2009). Titan's induced magnetosphere under non-ideal upstream conditions: 3D multi-species hybrid simulations. *Planetary and Space Science*, *57*(14–15), 2001–2015. https://doi.org/10.1016/j.pss.2009.08.010

Volwerk, M., Khurana, K., & Kivelson, M. (2007). Europa's Alfvén wing: Shrinkage and displacement influenced by an induced magnetic field. *Annales Geophysicae*, *25*(4), 905–914. https://doi.org/10.5194/angeo-25-905-2007

Zimmer, C., Khurana, K. K., & Kivelson, M. G. (2000). Subsurface Oceans on Europa and Callisto: Constraints from Galileo magnetometer observations. *Icarus*, *147*(2), 329–347. https://doi.org/10.1006/icar.2000.6456